Electrostatic modeling of cavities inside linear actuators

T A van Beek, J W Jansen, J van Duivenbode and E A Lomonova

Department of Electrical Engineering, Eindhoven University of Technology, Eindhoven, 5600MB, Den Dolech 2, The Netherlands

E-mail: t.a.v.beek@tue.nl

Abstract. This paper describes the modeling of two-dimensional electric fields inside linear actuators where cavities in the cooling environment are present. A semi-analytical model based on Fourier series is extended for cavities and incorporates the curvature of corners. The model shows good agreement with finite element analysis. The effect of position and sizes of the cavity are investigated as well as the curvature of the corners of the cavity.

1. Introduction

Increasing demands of the throughput of high-precision positioning systems require more powerful actuators in the positioning stages. To prevent the coils of these actuators from exceeding critical temperatures the coil array is mounted on a, electrically conductive, cooling environment which for safety reasons is connected to protective earth. However, cavities are present in the geometry of the cooling environment because of surface irregularities or mounting holes. The corners of the cavities introduce electric field enhancement, which can cause local dielectric breakdown if the breakdown strength of the insulation is exceeded. Besides the geometrical parameters of the corner, the electric field enhancement introduced by the corner is also determined by its curvature since a sharp corner would lead to an infinite electric field strength at the corner tip [1].

The modeling of the electric field distribution is usually performed by finite element or boundary element methods [2]. However, these methods are slow compared to analytical techniques such as conformal mappings [3] or Schwarz-Christoffel mappings [4]. Curvatures can be taken into account with these modeling techniques, however, due its parametric representation this is only possible for simple domains without loss of accuracy [5].

In this paper, a combination of Fourier modeling and a conformal mapping is proposed as modeling technique for the linear actuator configuration [6]. Globally, the field solution is obtained by Fourier modeling whereas locally the field solution near the curved corner is obtained by a conformal mapping of the curved corner. The derived field solution is validated with a 2-D finite element model.

2. Model formulation

The investigated linear actuator configuration is shown in Figure 1, where a coil is situated between an insulation layer and a cooling environment which inhibits cavities. The dimensions indicated in the figure and the material properties are given in Table 1. The configuration is divided in a number of regions as indicated in Figure 1 such that each region has homogenous material properties. By dividing the investigated configuration a boundary value problem is obtained which is solved based on boundary conditions. Furthermore, the periodicity present in the linear actuator configuration allows a computational reduction to one period and gives a fundamental frequency for the Fourier modeling. Fundamental frequencies for region I and II are given by

$$\omega^I = \frac{2\pi}{w_{per}} \quad \text{and } \omega^{II} = \frac{2\pi}{w_{cav}}. \tag{1}$$

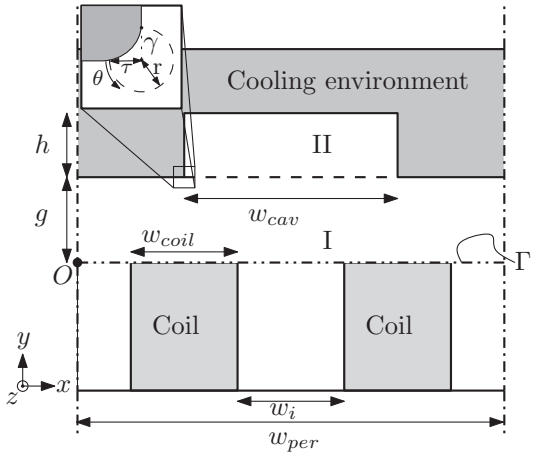

Figure 1: The linear actuator configuration in a Cartesian coordinate system with origin O

Table 1: Dimensions and material properties used in the linear actuator configuration

w_{coil}	10 [mm]	Width of the coil
w_{cav}	30 [mm]	Width of the cavity
w_{per}	40 [mm]	Width of the period
w_i	10 [mm]	Width of intercoil gap
g	5 [mm]	Height of the insulation gap
h	5 [mm]	Height of the cavity
ε_I	1	Relative permittivity of region I
ε_{II}	1	Relative permittivity of region II
V_p	1 [V]	Coil voltage wrt PE
V_e	0 [V]	Cooling environment voltage wrt PE
τ	100 [μm]	Curvature radius
N_I	91	Number of harmonics region I
N_{II}	21	Number of harmonics region II

2.1. Semi-analytical solution

Based on the electrostatic Maxwell equations and the assumption that the electric and the magnetic fields are decoupled, then $\nabla \times \vec{E} = 0$ and the electric field strength can be expressed by

$$\vec{E} = -\nabla\phi, \tag{2}$$

where ϕ is the electric scalar potential. Since it is assumed that no free charges are present in the materials, Gauss's law reduces to

$$\nabla \cdot \varepsilon\vec{E} = 0, \tag{3}$$

where ε is the relative permittivity of a material. By substituting Eq. 2 into 3 the Laplace equation is obtained for the electric scalar potential. Using the separation of variables the Laplace equation is solved. As a solution, a product of two function is obtained, one dependent on the x-direction and one on the y-direction.

$$\phi_k = a_0^k + \sum_{i=1}^{N}(a_i^k cos(\omega_i^k x) + b_i^k sin(\omega_i^k x))(c_i^k e^{\omega_i^k y} + d_i^k e^{-\omega_i^k y}), \tag{4}$$

where ω_i^k is the i-th spatial harmonic of the k-th region and N the number of spatial harmonics.

2.2. Boundary conditions

The field quantities in the different regions of the semi-analytical model are dependent on the boundary conditions. Regions I and II have a boundary at $y = 0$ and $y = g + h$, respectively. The electric scalar potential at these boundaries is defined by the environment. At $y = 0$, along path Γ, the electric scalar potental is subjected to a Dirichlet boundary condition which mimics the potential distribution of the coil and is given by

$$\phi_I\big|_{y=0} = \begin{cases} V_p & \frac{1}{2}w_i \geq x \geq w_{coil} + \frac{1}{2}w_i \\ -V_p & \frac{1}{2}(w_{per} + w_i) \geq x \geq w_{per} - \frac{1}{2}w_i \\ 0 & \text{else.} \end{cases} \tag{5}$$

At $y = g + h$, the electric scalar potential is defined by the cooling environment and given by

$$\phi_{II}\Big|_{y=g+h} = 0. \tag{6}$$

The boundary condition between region I and II is a combination of a Dirichlet and a continuous boundary condition. This combined boundary occurs between regions with unequal width and implies that both regions

have a different fundamental frequency. Observing the interface between region I and II, it is clear that for region II a continuous boundary is present at the interface with region I. Therefore, for region I a continuity is required at the interval with region II. For the remainder of the interface of region I, a Dirichlet boundary is present which is imposed by the cooling environment. The boundary conditions between region I and II are given by

$$\phi_I = \begin{cases} \phi_{II}\big|_{y=g} & 0.5\, w_{per} - dx \leq x < 0.5\, w_{per} + dx, \\ 0 & \text{else}, \end{cases} \tag{7}$$

$$\varepsilon_{II} \frac{\partial \phi_{II}}{\partial y} = \varepsilon_I \frac{\partial \phi_I}{\partial y}\bigg|_{y=g}. \tag{8}$$

The combined boundary conditions in Equation 7 and 8 can be solved using mode-matching [7].

2.3. Curvature of corners

The semi-analytical model as described in Section 2.1 is unable to model the curvature of rounded elements since the system is solved in a Cartesian coordinate system. This results in solutions that are globally accurate but locally inaccurate in the neighbourhood of a rounded element. To incorporate the curvature of rounded element a separate model calculates the electric potential due to an unbounded profile. The calculation of the electric potentials due to the unbounded profile are performed by a conformal mapping. The conformal map of the unbounded profile is given by

$$z = k[(w+a)^{\frac{1}{\alpha}} + (w-a)^{\frac{1}{\alpha}}], \tag{9}$$

where

$$z = x + iy \qquad \text{corresponding to the real geometry,} \tag{10}$$

$$w = u + iv \qquad \text{where v is the electric potential,} \tag{11}$$

with $k = \frac{1}{2}$, $a = 2^{\alpha-1}$ and $\alpha = \frac{2}{3}$ for a straight corner. The total potential distribution, ϕ_t, is obtained by combining the solutions of the semi-analytical model,ϕ_{sa}, and the unbounded profile,ϕ_{unb}, and is given by

$$\phi_t = \lambda \tau^{\alpha} \phi_{unb} \qquad \text{for } r \leq \tau, \tag{12}$$

$$\phi_t = \phi_{sa} + \lambda \tau^{\alpha} \phi_{unb} \qquad \text{for } r > \tau, \tag{13}$$

where λ represents the singularity factor, as in [6], and τ the curvature radius. The singularity factor is obtained by performing a weighted line integral in the semi-analytical model from border to border of the sharp corner. The singularity factor is given by

$$\lambda = \frac{4}{3\pi} \tau^{-\alpha} \int_0^{\frac{3\pi}{2}} \phi_{sa}(\tau, \theta) sin(\alpha\theta) d\theta, \tag{14}$$

where θ is the angle from border to border of the corner. In this model the electric field strength is obtained numerically.

3. Verification of the combined model

To validate the results of the combined model, the linear actuator configuration in Figure 1 is modeled with 2-D finite element method using Cedrat FLUX2D [8] for the parameters given in Table 1. Near the corner, the electric field strength is compared along path γ, parallel to the y-axis and starting from the original position of the sharp corner and ending at the cooling environment. The electric field strength in the y-direction along path γ is shown in Figure 2a for both the combined model and the Finite Element Model (FEM). In this figure Q is the normalized position along γ with respect to the curvature radius. The average discrepancies between the model and FEM for curvature radii, τ, of 0.1, 1 and 3 [mm] are 19, 17 and 10 [%], respectively. Furthermore, it is observed that for a curvature radius of 3 [mm] the discrepancy increases to above 20 [%] near the starting point of path γ. This is due to the conformal mapping presented in Equation 9, which assumes a constant potential on its mapped electrodes. For small curvatures this is a valid assumption but for larger curvatures this is not the case and the discrepancy at points far from the corner increases for increasing curvature radii.

The selected harmonic numbers, N_I and N_{II}, are sufficient for these simulations since tripling the number of harmonics resulted in less than 1 [%] change in the first 9 harmonic coefficients.

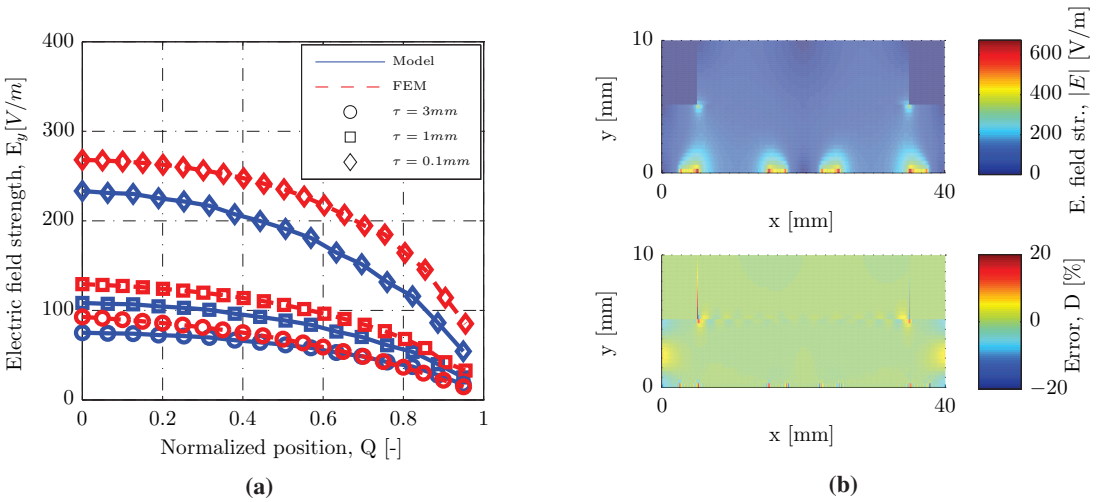

(a) **(b)**

Figure 2: (a) Electric field of the combined model and FEM along path γ for radii. (b) Electric field and the discrepancy between FEM for the combined model for $w_{cav} = 30[mm]$ and $\tau = 0.1[mm]$.

In Figure 2b the potential distribution and the discrepancy with the finite element model of a periodical section of the linear actuator configuration is shown. The discrepancy, D, is calculated as

$$D = 100\frac{|E_t| - |E_{FEM}|}{max(|E_t|)}, \tag{15}$$

where E_t and E_{FEM} are the electric field strength of the combined model and FEM, respectively. The discrepancies near the corners are below 15 [%], this is lower than the discrepancies as obtained from Figure 2a. This is due to meshsize of the results, which is larger than the curvature of the corner. Furthermore, the discrepancies, up to 20 [%], on the sides of the cavity are caused by a slight difference in cavity width between the combined model and FEM (30.02 vs 30 [mm]) to allow numerical convergence of the semi-analytical model.

4. Conclusion

In this paper, a conformal mapping and semi-analytical model combined presents the electric potential distribution of a periodical section inside a linear actuator where cavities are present. The local potential distribution near rounded elements is taken into account by a conformal mapping of an unbounded profile. Globally, the electric potential distribution inside the linear actuator is modeled using the Fourier modeling technique extended with mode-matching. The field solutions of the combined model are verified with 2-D finite element analyses for different curvature radii of the corner of the cavity. For large curvature radii the average discrepancy is low, 10 [%], compared to smaller curvature radii, 19[%]. However, for large curvature radii the discrepancy far from the corner increases to above 20 [%]. Therefore, this model is suited to investigate linear actuator configurations with relative small curvatures.

References

[1] Langton N and Smith M 1977 *Electrical Engineers, Proceedings of the Institution of* **124** 277–284 ISSN 0020-3270
[2] Lerch R, Kaltenbacher M, Landes H, Peipp R and Simkovics R 2002 *Sensors, 2002. Proceedings of IEEE* vol 2 pp 1233–1238 vol.2
[3] Brenna M, Martinelli F and Zich R 2004 *Mathematical Methods in Electromagnetic Theory, 2004. 10th International Conference on* pp 277–279
[4] O'Connell T and Krein P 2010 *Energy Conversion, IEEE Transactions on* **25** 606–618 ISSN 0885-8969
[5] Delillo T K *SIAM Journal on Numerical Analysis* **31** pp. 788–812
[6] Krahenbuhl L, Buret F, Perrussel R, Voyer D, Dular P, Peron V and Poignard C 2011 *Journal of Microwaves, Optoelectronics and Electromagnetic Applications* **10** 66 – 81 ISSN 2179-1074
[7] Gysen B, Meessen K, Paulides J and Lomonova E 2010 *Magnetics, IEEE Transactions on* **46** 39–52 ISSN 0018-9464
[8] Cedrat 2014 *FLUX 11.2.2 User's Guide* (Meylan: France)